

Design of a pulse-type strain gauge balance for a long-test-duration hypersonic shock tunnel

Y. Wang¹ · Y. Liu¹ · Z. Jiang¹

Received: 25 October 2014 / Revised: 4 December 2015 / Accepted: 16 December 2015 / Published online: 9 January 2016
© Springer-Verlag Berlin Heidelberg 2016

Abstract When the measurement of aerodynamic forces is conducted in a hypersonic shock tunnel, the inertial forces lead to low-frequency vibrations of the model, and its motion cannot be addressed through digital filtering because a sufficient number of cycles cannot be obtained during a tunnel run. This finding implies restrictions on the model size and mass as the natural frequencies are inversely proportional to the length scale of the model. Therefore, the force measurement still has many problems, particularly for large and heavy models. Different structures of a strain gauge balance (SGB) are proposed and designed, and the measurement element is further optimized to overcome the difficulties encountered during the measurement of aerodynamic forces in a shock tunnel. The motivation for this study is to assess the structural performance of the SGB used in a long-test-duration JF12 hypersonic shock tunnel, which has more than 100 ms of test time. Force tests were conducted for a large-scale cone with a 10° semivertex angle and a length of 0.75 m in the JF12 long-test-duration shock tunnel. The finite element method was used for the analysis of the vibrational characteristics of the Model-Balance-Sting System (MBSS) to ensure a sufficient number of cycles, particularly for the axial force signal during a shock tunnel run. The higher-stiffness SGB used in the test shows good performance, wherein the frequency of the MBSS increases because of the stiff construction of the balance. The experimental results are compared with the data

obtained in another wind tunnel and exhibit good agreement at $M = 7$ and $\alpha = 5^\circ$.

Keywords Hypersonic shock tunnel · Force measurement · Strain gauge balance

1 Introduction

For the conventional hypersonic shock tunnel, mechanical vibration of the model-balance-sting system (MBSS) occurs and cannot be damped during a shock tunnel run because of the short test time (generally $500 \mu\text{s}$ – 20 ms) [1–4]. Therefore, if an averaging method is adopted during signal processing, then at least five cycles of balance signal, with the lowest vibrational frequency of the MBSS, should be observed during the test time to obtain better measurement results [2]. Sometimes, the lowest natural frequency of 1 kHz is required for a test time of typically 5 ms in the shock tunnel. The higher the natural frequencies, the better the justification for the neglected acceleration compensation. For such test conditions, many balance experts proposed several special balances to measure aerodynamic forces in a shock tunnel [5–14].

Difficulties regarding the effective test time can be alleviated in the JF12 hypersonic shock tunnel, which can provide a test time of more than 100 ms and is capable of duplicating hypersonic flight conditions [15]. Therefore, a stiff construction balance, which is a traditional internal SGB, was used in the long-test impulse facility because of its mature technology, simple structure, and low cost. In this study, four models of the SGB were proposed and the structures were optimized by using the finite element method (FEM). The computational and experimental results show that the SGB still covers a large scope for structural improvement to obtain

Communicated by K. Hannemann and A. Higgins.

✉ Y. Wang
wangyunpeng@imech.ac.cn

¹ State Key Laboratory of High Temperature Gas Dynamics (LHD), Institute of Mechanics, Chinese Academy of Sciences (CAS), Beijing 100190, China

higher measurement accuracy. Based on the finite element analysis (FEA), one of the four models is selected and a prototype is built for the measurement of aerodynamic forces in the JF12 hypersonic shock tunnel.

All aspects of balance technology must be investigated to design and construct an SGB model that can meet the aforementioned demands. In this study, only the structure of the SGB is considered. From the point of view of the structure, the demands on the balance are (1) low interference between different loads; (2) high stiffness; (3) low stress level at the strain gauge positions and related parts, and (4) capability of tolerating errors from temperature gradients. Of these demands, the important properties of interference and stiffness (natural frequency) are investigated in this study. Therefore, the goal of this study is to increase the measurement accuracy of the traditional SGB in a hypersonic shock tunnel, particularly the axial force component, by improving and optimizing the structure of the measurement element.

2 Design and optimization of the SGB

2.1 Several designs

Four SGB models were proposed to compare their performance and capability. Figure 1 shows the three-dimensional model diagrams. Table 1 lists the balance dimensions of the four models. Table 2 presents the maximum forces and moments (limited loads) for these models. In the present study, the larger axial force was considered for the test in the hypersonic shock tunnel. All three components (axial force, normal force, and pitching moment) of the SGB, except for model B, can measure six components. The structures of models A and B, which are considered tentative designs, are the traditional types used in conventional high-speed wind tunnels [16]. These structures were tested to determine whether this type of SGB can be used in a hypersonic shock tunnel.

Based on models A and B, the SGB structure is improved and model C is proposed. Model D is designed through further optimization of the structure. Model C has a cage-type structure and only one rectangular beam on one side of the calibration center, which will significantly increase the stiffness of the SGB. In this type, the structure of the element needed to measure the axial force becomes more complicated.

2.2 Axial force element

Compared with other measurement elements, the axial force element is difficult to design because of its complicated structure. A considerable number of geometries were examined to construct an appropriate measurement element of the

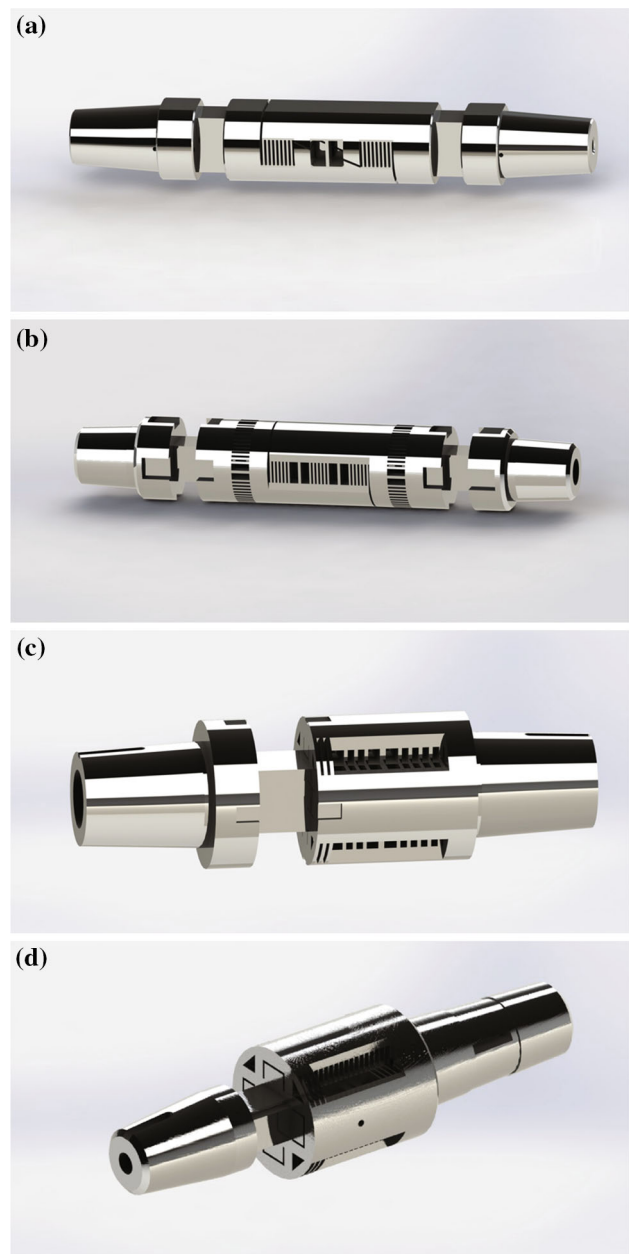


Fig. 1 Models of the investigated balance designs. **a** Model A. **b** Model B. **c** Model C. **d** Model D

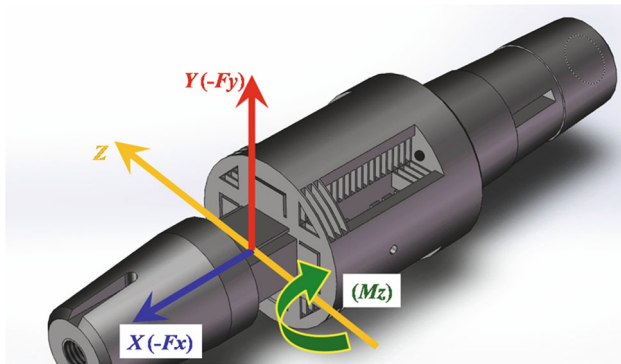
Table 1 Balance dimensions (mm)

Model	Diameter (D)	Length (L)
A	44	264
B	40	246
C	50	175
D	53	202.5

axial force, which has higher precision and accuracy. For the impulse facility, such as the hypersonic shock tunnel, several researchers measured the axial force by using a special bal-

Table 2 Specified load ranges (N, Nm)

Model	F_x	F_y	F_z	M_x	M_y	M_z
A	1000	3000	–	–	–	100
B	1000	3000	3000	50	100	100
C	1500	4000	–	–	–	150
D	1000	2000	–	–	–	100

**Fig. 2** Definition of the coordinate system in the case of model D

ance, e.g., the accelerometer balance [7], stress wave force balance [8–10], free-flight measurement technique [11–13], and compensated balance [14], because the test time is short. Thus, a sufficient number of cycles cannot be obtained during a shock tunnel run. If the test time is more than 100 ms, then the SGB with an optimized structure can be used for the force test in the hypersonic shock tunnel.

Based on the aforementioned analyses, we attempted to design different structures of the axial force element and conduct a series of finite element computations in the case of model D. Figure 2 presents the definition of the coordinate system. The normal force is defined as the negative component of the total force projected onto the Y -axis; the axial force is defined as the negative component of the total force projected onto the X -axis; and the pitching moment is defined as the component of the total moment projected onto the Z -axis.

Figure 3 illustrates nine geometries of the axial force element with three different types, namely, I-beam, bending beam I, and bending beam II. The comparison of these three beams by FEM computation shows that the structure of bending beam II has small interferences, which are less than 5%. In the present study, the interference is the strain output of the axial force element when only the normal force (or pitching moment) was applied to the balance moment center.

Similarly, in the three cases of bending beam II, case (1) shows the smallest interference in the presence of a load, which is the normal force or pitching moment acting on the moment center. At the same time, case (1) has the largest strain output, $336 \mu\epsilon$, while the case (a) is only $64 \mu\epsilon$. Case (1) also has the highest sensitivity for force measurement.

Therefore, only case (1) of model D is considered in the subsequent analyses.

2.3 Stress and strain analysis

2.3.1 Material property

The properties of the balance material for linear stress analysis are as follows:

Young's modulus of elasticity, $E = 1.8725 \times 10^{11}$ Pa;
Poisson's ratio, $\nu = 0.4049$;
Yield strength, $\sigma_b = 1.862 \times 10^9$ Pa.

2.3.2 Strength analysis and strain calculation

Strength check and strain analysis of the SGB (model D) were conducted in the present study to assess security and applicability. On one hand, the computational results show that the strength of model D meets the design requirement and the structure is safe under the present maximum load. Table 3 shows the maximum von Mises stress results for three individual load components by FEM simulation. The maximum von Mises stress, which is 446 MPa, also occurs when the three load components are applied together at the moment center.

On the other hand, the strain analysis results show that the present structure [case (1) of model D, as shown in Fig. 3i] has the highest measurement sensitivity. Table 4 shows the strain results at the location of the strain gauge for the individual components.

2.4 Modal analysis

Modal analysis was conducted to understand the structural behavior of the four models. The natural frequencies and mode shapes were calculated by the FEM. The computational results of the modal analysis show that model D has the highest natural frequency, which is more than 850 Hz (see Table 5). Based on the higher natural frequency of the balance, the stiffness of the MBSS can be further increased. As a result, more cycles can be obtained during a shock tunnel run. The experimental results presented in Sect. 3 verified this issue. Figure 4 shows the first three mode shapes. The first two modes are bending around the Z - and Y -axes. The third mode is axial and located in the X -axis, which implies that the output signal of the axial force will have a higher frequency in the force test using the hypersonic shock tunnel.

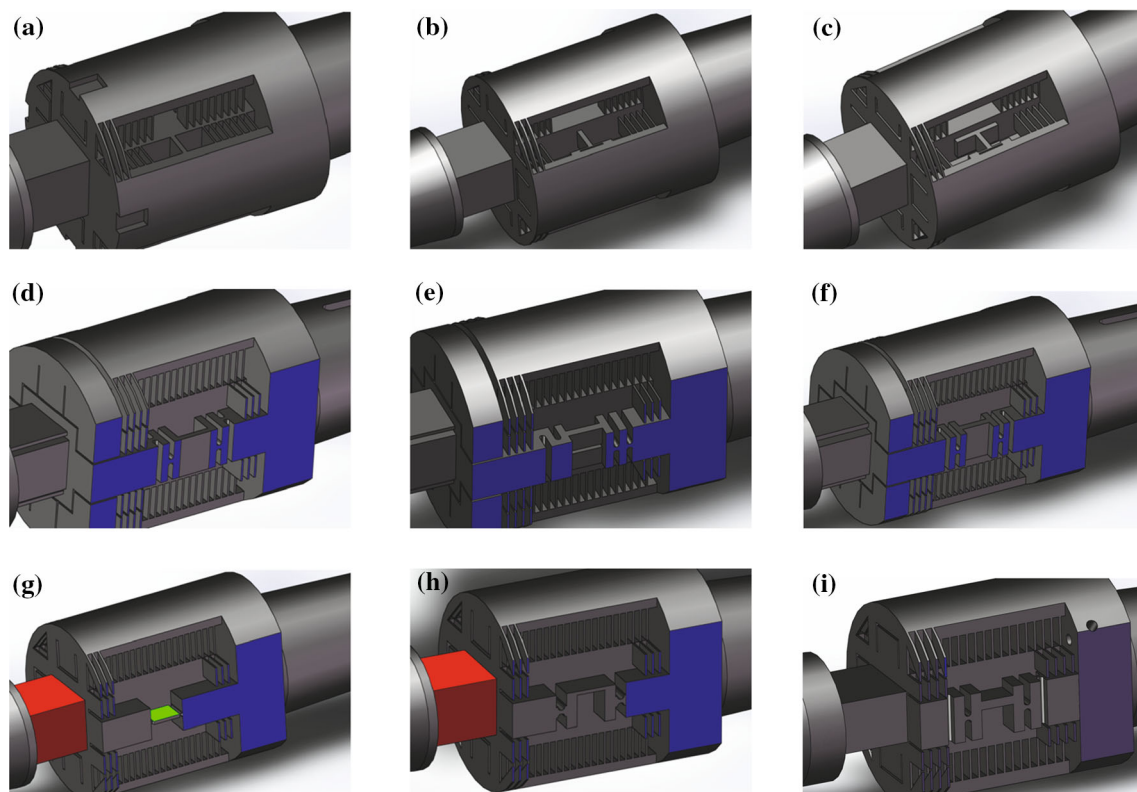


Fig. 3 Different geometries for the axial force element in the case of model D. **a** I-beam: parallel to the y - z plane. **b** I-beam: parallel to the y - z plane. **c** I-beam: parallel to the y - z plane. **d** Bending beam I: parallel to the x - y plane. **e** Bending beam I: parallel to the x - y plane. **f** Bending

beam I: parallel to the x - y plane. **g** Bending beam II: parallel to the x - z plane. **h** Bending beam II: parallel to the x - z plane. **i** Bending beam II: parallel to the x - z plane

Table 3 Maximum von Mises stress for three individual load components

Load	F_x	F_y	M_z
Limit loads (N, Nm)	1000	2000	100
Maximum stress, σ_{\max} (MPa)	154	312	173

Table 4 Maximum strain for three individual load components

Load	F_x	F_y	M_z
Limit loads (N, Nm)	1000	2000	100
Maximum strain, ε_{\max} ($\mu\varepsilon$)	823	1664	923
Averaged strain, ε_{ave} ($\mu\varepsilon$)	336	595	722

Table 5 First three frequencies by modal analysis (Hz)

Mode	Model A	Model B	Model C	Model D
1	335.38	281.35	747.18	878.08
2	405.91	289.63	757.31	880.64
3	1085.6	1281.4	2358.6	1907.4

2.5 Balance calibration

The calibration loads are 1920 N, 96 Nm, and 960 N for the normal force, pitching moment, and axial force, respectively.

The moment center, which is the center of the rectangular beam, was selected as the reference center for the static calibration.

The multicomponent loading method was employed in the present study for the calibration of the present pulse-type SGB. In the multicomponent loading calibration process, every component is simultaneously loaded under different load combinations. An equation describing the relationship between the load and the balance signal can be constructed for every loading, with the unknown coefficients of the calibration formula. The calibration formula of balance is obtained by solving a set of calibration equations [17].

The mathematical modeling of the calibration relates the aerodynamic component F to the functions of the strain gauge bridge reading R (see 1). The system is multivariate and consists of a linear combination of nine functions of R . These functions are called basis functions and correspond to R_1 , R_2 , R_3 , R_1R_1 , R_1R_2 , R_1R_3 , R_2R_2 , R_2R_3 , and R_3R_3 . aerodynamic components. The model's dependence on its parameters a and b is linear. Each of the three aerodynamic components has nine adjustable parameters. The dependence of the model on its parameters a and b is linear.

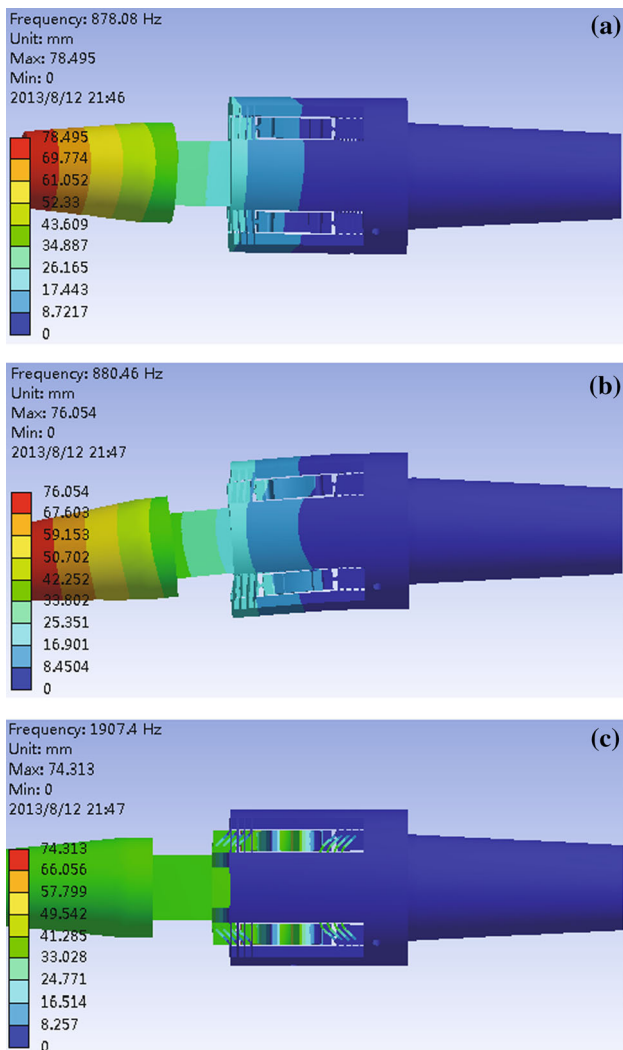


Fig. 4 First three mode shapes (top view) in the computational coordinate. **a** First mode shape bending along the x -axis. **b** Second mode shape bending along the y -axis. **c** Third mode shape, axial

$$F_i = \sum_{j=1}^3 a_{i,j} R_j + \sum_{j=1}^3 \sum_{k=j}^3 b_{i,j,k} R_j R_k \quad (1)$$

At each of the 76 loadings (total loading number), the bridge outputs are read several times and the mean values and standard deviations are computed. Table 6 shows the calibration matrix, where the small interferences between bridges are denoted by the values of the cross-product terms.

The mean squared error was computed by the following equations.

$$\delta_i = \sqrt{\sum_{j=1}^m \frac{(P_{j,i} - F_{j,i})^2}{m - 1}} \quad (2)$$

$$\sigma_i = \frac{\delta_i}{F_{L_i}} \times 100\% \quad (3)$$

Table 6 The calibration matrix

	F_y	M_z	F_x
F_y	1.8948E+03	4.3758E-06	3.1455E-03
M_z	-5.1255E-01	1.2899E+01	2.0600E-01
F_x	1.2730E-03	1.9250E-04	2.0492E+02
F_y^2	3.1270E-07	5.3816E-08	-6.5705E-07
M_z^2	-5.9041E-05	3.7358E-06	3.0362E-05
F_x^2	1.1324E-06	2.3377E-08	-1.5179E-07
$F_y * M_z$	9.2902E-06	4.8693E-07	-5.1159E-05
$F_y * F_x$	-2.8996E-07	-2.2484E-08	2.3994E-07
$M_z * F_x$	1.9249E-05	7.7543E-07	1.4646E-06

Table 7 The mean squared error of the static calibration

	F_y	M_z	F_x
σ (%)	0.26	0.12	0.03
ϵ (%)	0.77	0.36	0.08

Table 8 The precision of the balance

Load	F_y	M_z	F_x
Precision (%)	0.03	0.05	0.03

$$\epsilon_i = 3 \times \sigma_i, \quad (4)$$

where

$$i = 1, 2, 3;$$

$m = 21$, which is the number of data points;

$P_{j,i}$ represents the measured component loads;

$F_{j,i}$ is the applied load, which corresponds to the weight applied to the calibration system;

F_{L_i} is the limited loads (design loads);

δ_i is the absolute error;

σ_i is the relative error;

ϵ_i is the limit error.

Tables 7 and 8 show the calibration performance and mean squared error of the static calibration and the precision of the balance, respectively. The present structure of the balance shows that the accuracy and the combined loading repeatability in the static calibration are good.

3 Force measurement

Model D, with the structure of bending beam II (see Fig. 3i), was processed, and the calibration experiment was conducted to assess the structural performance of the present SGB.

3.1 Test facility and model

The force tests were conducted in the JF12 hypersonic shock tunnel, which is a long-test-duration impulse facility approximately 278 m in length with a nozzle exit diameter of 2.5 m. This impulse facility is capable of reproducing air flows of 100 ms test duration for Mach 5–9 at 30–40 km altitude to meet the requirements of full-scale testing of integrated hypersonic vehicles and investigating the fundamental physical issues in hypersonic and high-temperature gas dynamics [15]. In the tests, the average stagnation pressure is 2.5 MPa and the average stagnation temperature is 2200 K. These conditions resulted in an average free-stream Mach number of 7 and an average unit Reynolds number of approximately 0.8×10^6 per meter. The model was supported by a tail sting mounted on the support mechanism in the test section. The tests were conducted at nominal angles of attack 5° with a zero sideslip angle (see Table 9).

A cone made of aluminum alloy with a length of 0.75 m and a 10° semivertex angle was employed in the test. The cone is a standard model and has a considerable amount of test data. Table 10 shows the reference area and dimensions of the models, including the models of the China Academy of Aerospace Aerodynamics and the National Aeronautics and Space Administration (NASA), where CAS' cone is the largest.

Figures 5 and 6 show the test model and the SGB, which was model D in the aforementioned description, used in the force test utilizing the JF12 hypersonic shock tunnel.

Prior to the shock tunnel run, the three-dimensional design of the MBSS is modeled. A series of computations, including the static structure, dynamics, and modal analysis, is conducted by using FEA. The numerical results can be used to estimate the experimental results, such as the MBSS vibrational frequency and cycle number, during the limited test time. Figure 7 shows the three-dimensional modeling of the MBSS by using FEA.

Table 9 Test flow condition

M_∞	α ($^\circ$)	T_0 (K)	P_0 (MPa)	Re (1/m)
7	5	2200	2.5	0.80×10^6

Table 10 Dimensions of the cones employed in different wind tunnels

Test wind tunnel	Length (m)	Reference area (m^2)	Weight (kg)
JF12	0.75	0.0549	6.9
FD-03	0.14178	0.00196	–
Langley 11 inch	0.0855	0.0007	–

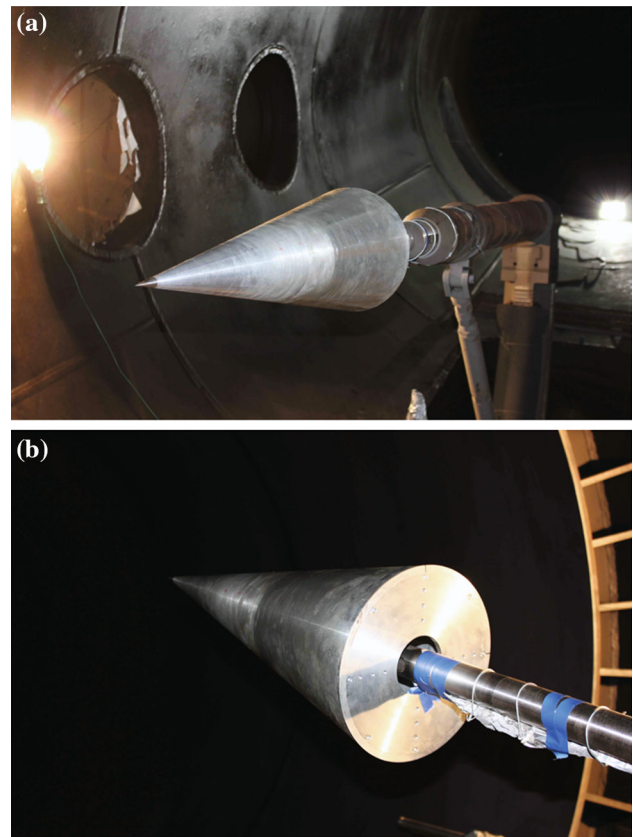


Fig. 5 The cone is shown in the JF12 hypersonic shock tunnel (MBSS). **a** Side view. **b** Base view



Fig. 6 Photo of the present SGB

The first six mode shapes and frequencies are shown in Fig. 8. The vibrations of first, second, and fifth modes have relatively large effects on the balance's signals during force measurement because the present SGB has three components (axial force, normal force, and pitching moment). Therefore, the present SGB cannot be used to evaluate the effect of side force on the test. However, the present test has no sideslip angle setting. Thus, the aforementioned modes cannot be easily excited, or their effects can be ignored. The third, fourth,

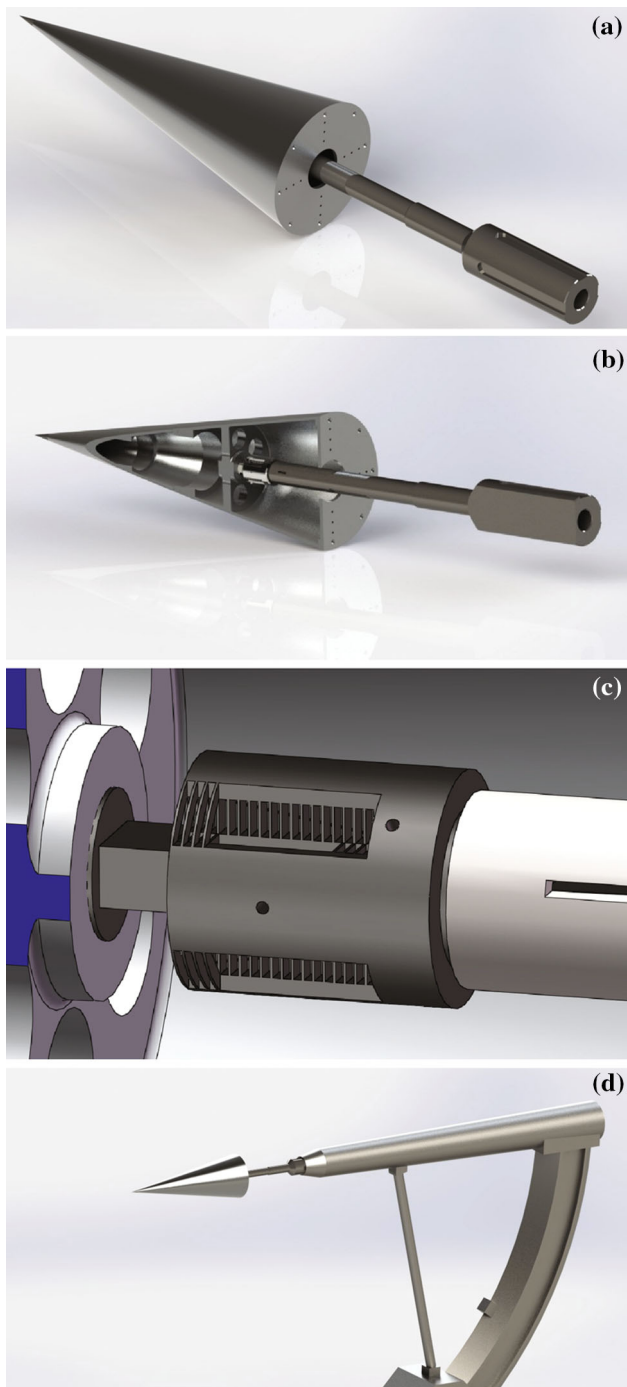


Fig. 7 Three-dimensional modeling of the MBSS by using FEA. **a** Side view. **b** Cross section. **c** Location of the new SGB. **d** Overview of MBSS

and sixth modes are bending along the Z-axis, which mainly affect the output signal of the normal force. These effects will be fully analyzed in the subsequent section.

3.2 Balance signal processing

Force tests were conducted for the dynamic calibration of this new balance by using a standard model, which is a cone with

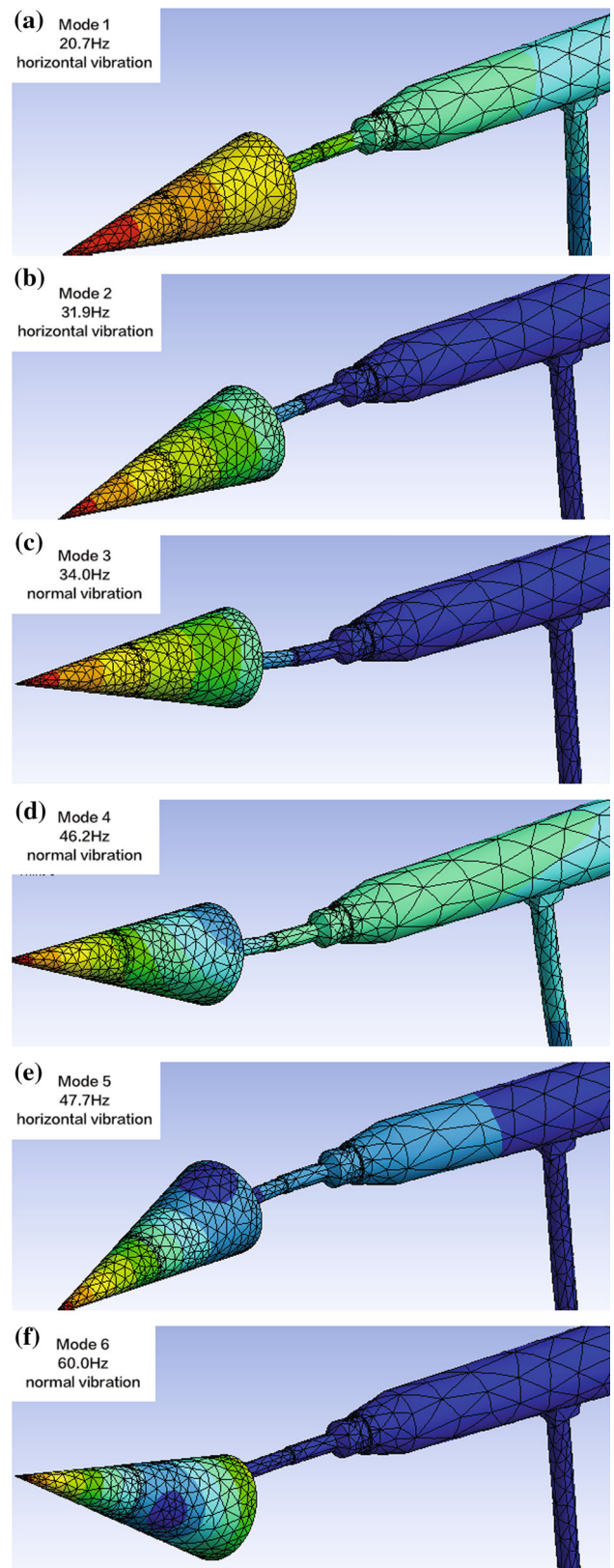


Fig. 8 Modal analysis. **a** Mode 1. **b** Mode 2. **c** Mode 3. **d** Mode 4. **e** Mode 5. **f** Mode 6

a 10° semivertex angle, in the JF12 hypersonic shock tunnel. The arithmetic mean was used for the averaging process of the balance signal.

Figure 9 shows the pitot pressure variation at the nozzle exit. The test time is clearly more than 100 ms based on the time history of the pitot pressure. The balance signals are shown in the figures. The signal frequencies are different for each component, and the integral cycle number is selected when the test data are averaged. Therefore, the balance signals for each component were processed with different time ranges during the same test time.

In Fig. 10, two voltage signals of the normal force are compared to show the repeatability of the SGB, where the same vibrational characteristics and cycle number can be observed. The signals were processed at the time ranges of 96 and 91 ms. Two frequencies, 30.52 and 61.04 Hz, were obtained by using the fast Fourier transform analysis in Fig. 10a. Based on the description presented in the previous section, two frequencies, 34 and 60 Hz (which are close to the other two frequencies previously mentioned) can be obtained from the modal analysis. The FEA successfully predicted the vibration performance of the MBSS in the normal direction. A 30-Hz frequency indicates the existence of three cycles within 100 ms. Therefore, according to the FEA results, at least three cycles can be obtained during a test run. Based on the FEM computation, the SGB structure was continuously improved, such that it has sufficient stiffness and sensitivity, particularly for the axial force structure.

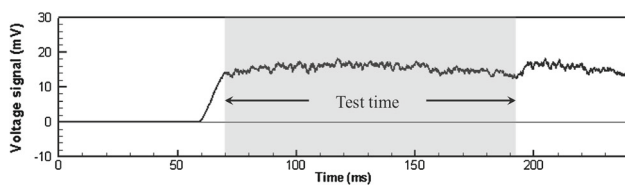


Fig. 9 Time history of pitot pressure

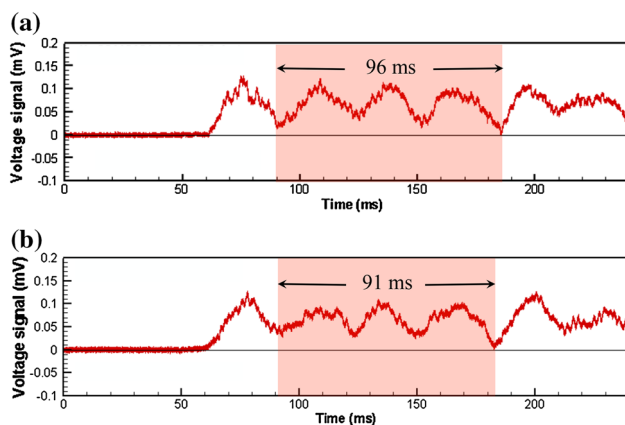


Fig. 10 Voltage signals of the normal force (two tests with the same conditions). **a** No. 1 signal. **b** No. 2 signal

The balance signals of the axial force are shown in Fig. 11. Figure 11a, b was obtained by using the present SGB, and a high frequency can be observed during the test time. In this case, the processing times are 87 and 81 ms, which are from approximately $t = 105$ to 190 ms in Fig. 11. The large oscillations of the normal force and the pitching moment have been noted to have slight effects on the axial load signal. The output signals were also compared with that of the other SGB used in the JF12 shock tunnel (see Fig. 11c). Notably, the present design has a larger output, i.e., a higher sensitivity for the force measurement of the axial force under the same test conditions and same setting of the data acquisition system.

Figure 12 shows the balance signal of the pitching moment, and only one cycle (the processing times are 62

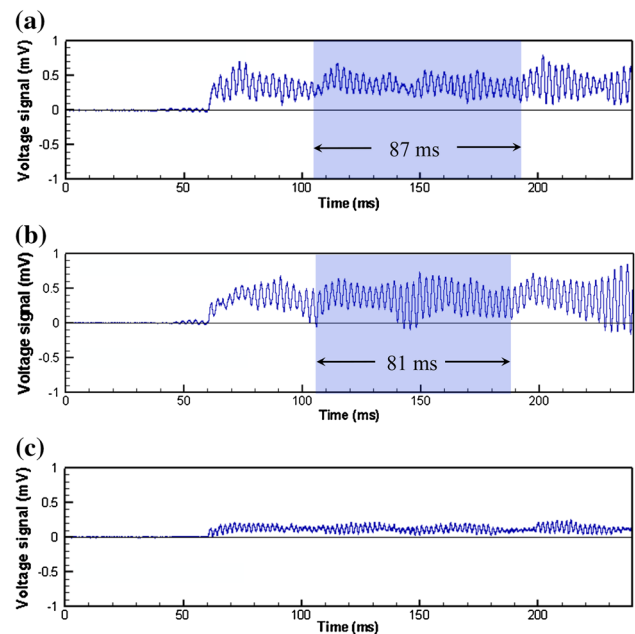


Fig. 11 Voltage signals of the axial force. **a** No. 1 signal. **b** No. 2 signal. **c** No. 3 signal by the other SGB

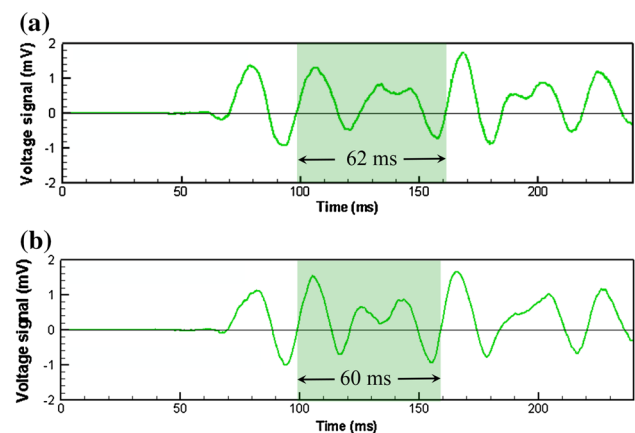


Fig. 12 Voltage signals of the pitching moment. **a** No. 1 signal. **b** No. 2 signal

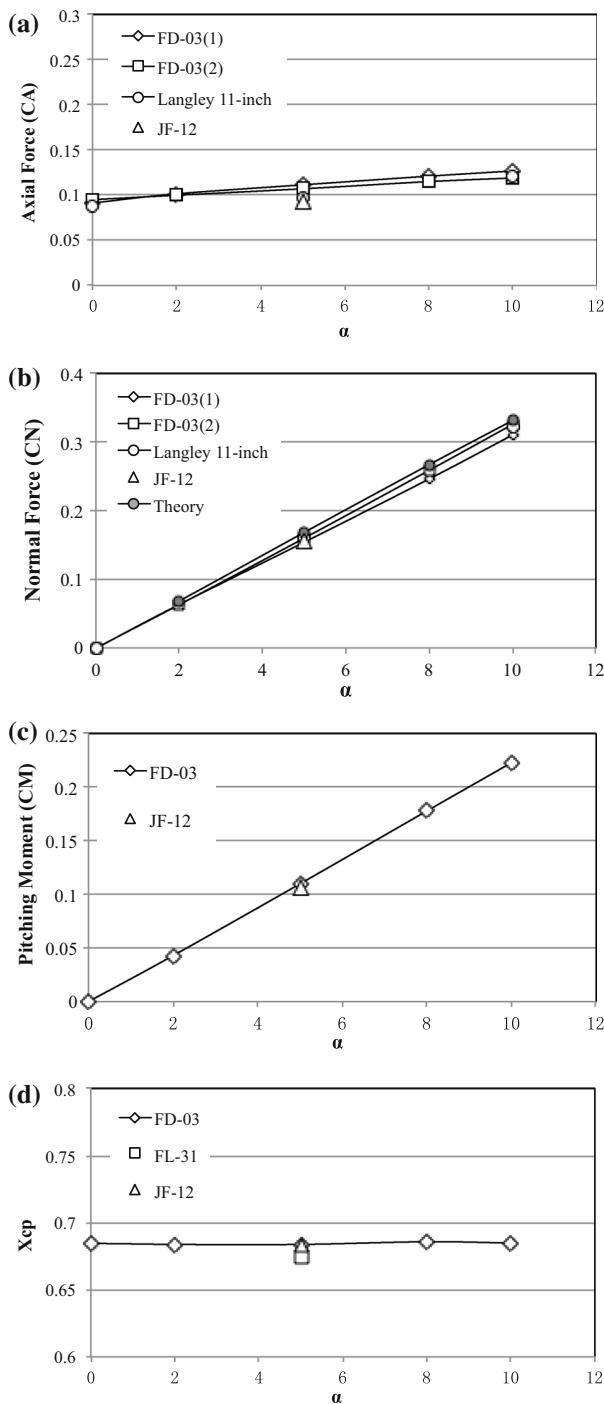


Fig. 13 Comparison of the aerodynamic coefficients at $M \approx 7$. **a** Axial force. **b** Normal force. **c** Pitching moment. **d** Pressure center

and 60 ms in the two tests) was observed during the test time because of the more complex vibrational mode. Therefore, the measurement capability of the axial force is evidently better than that of the normal force and the pitching moment in the force test using the present SGB.

Table 11 Precision of the test data obtained in the JF12 shock tunnel

σ_{CN}	σ_{CM}	σ_{CA}	$\sigma_{X_{cp}}$
0.242 %	0.186 %	0.537 %	0.283 %

3.3 Test results and discussion

Figure 13 shows the comparison of the test results and the data obtained by other conventional hypersonic wind tunnels (in the present study, the theoretical result was obtained on the basis of Cheng’s cone theory [18]). The results are consistent with the data acquired by the Langley 11 in. ($T_0 = 630$ K) [19,20] and the other wind tunnels. In NASA’s case, the Mach number was 6.8 and the Reynolds number was 0.81×10^6 . Compared with NASA’s data, the normal and axial force coefficients decreased by 2.61 and 4.69 %, respectively. For the hypersonic shock tunnel and the large test model, based on the aforementioned flow conditions, the test results are considered to be acceptable.

At the same time, good repeatability was observed during shock tunnel testing (see Table 11). Equation 5 is employed to calculate the standard deviation σ .

$$\sigma_X = \sqrt{\frac{\sum_{i=1}^n (X_i - \bar{X})^2}{n - 1}} \tag{5}$$

In Table 11, X is the arithmetic average value of n tests, with $n = 5$ in the present study.

4 Summary

A pulse-type SGB with three components was designed and optimized by using FEM. Based on the structural complexity of the axial element, the main objective of this study was to improve the axial force response and its measurement accuracy. The new SGB was employed for the force test of a calibration model in the JF12 large-scale shock tunnel. The test results showed the good structural performance of the new SGB, particularly its capability of axial load measurement. Through structural optimization, large oscillations of the normal loads have only a slight effect on the axial load signal, which ensures balance within an optimized structure suitable for the force test in a long-test-duration hypersonic shock tunnel. FEA was employed for the vibration analysis of the MBSS and successfully predicted the cycle number of the balance signal.

Acknowledgments The force tests were conducted in collaboration with Prof. W. Zhao and Dr. C. Yuan of the Institute of Mechanics. Prof. Z. Bi and Engineer J. Liu of CAAA gave us good advice on the design of the SGB. We are grateful for their cooperation. This study was supported

by the National Natural Science Foundation of China (Project Number 11302232).

References

1. Arrington, P.J., Joiner, R.J., Henderson, A.J.: Longitudinal characteristics of several configurations at hypersonic mach numbers in conical and contoured nozzles. NASA TN D-2489 (1954)
2. Bernstein, L.: Force measurement in short-duration hypersonic facilities. AGARDograph No. 214 (1975)
3. Naumann, K., Ende, H., Mathieu, G., George, A.: Millisecond aerodynamic force measurement with side-jet model in the ISL shock tunnel. AIAA J. **31**, 1068–1074 (1993)
4. Naumann, K., Ende, H.: A novel technique for aerodynamic force measurements in shock tubes. AIP Conf. Proc. **208**, 653–658 (1990)
5. Joarder, R., Jagadeesh, G.: A new free floating accelerometer balance system for force measurements in shock tunnels. Shock Waves **13**, 409–412 (2003)
6. Saravanan, S., Jagadeesh, G., Reddy, K.P.J.: Aerodynamic force measurement using 3-component accelerometer force balance system in a hypersonic shock tunnel. Shock Waves **18**, 425–435 (2009)
7. Sahoo, N., Mahapatra, D.R., Jagadeesh, G., Gopalakrishnan, S., Reddy, K.P.J.: An accelerometer balance system for measurement of aerodynamic force coefficients over blunt bodies in a hypersonic shock tunnel. Meas. Sci. Technol. **14**, 260–272 (2003)
8. Robinson, M.J., Schramm, J.M., Hannemann, K.: Design and implementation of an internal stress wave force balance in a shock tunnel. CEAS Space J. **1**, 45–57 (2011)
9. Sanderson, S.R., Simmons, J.M., Tuttle, S.L.: A drag measurement technique for free-piston shock tunnels. AIAA Paper 91–0540 (1991)
10. Mee, D.J., Daniel, W.J.T., Simmons, J.M.: Three-component force balance for flows of millisecond duration. AIAA J. **34**(3), 590–595 (1996)
11. Tanno, H., Komuro, T., Sato, K., Fujita, K., Laurence, S.J.: Free-flight measurement technique in the free-piston shock tunnel HIEST. Rev. Sci. Instrum. **85**, 045112 (2014)
12. Tanno, H., Komuro, T., Sato, K., Itoh, K., Yamada, T.: Free-flight tests of reentry capsule models in free-piston shock tunnel. AIAA Paper 2013–2979 (2013)
13. Laurence, S.J., Karl, S.: An improved visualization-based force-measurement technique for short-duration hypersonic facilities. Exp. Fluids **48**, 949–965 (2010)
14. Marineau, E., MacLean, M., Mundy, E., Holden, M.: Force measurements in hypervelocity flows with an acceleration compensated strain gage balance. J. Spacecr. Rockets **49**(3), 474–482 (2012)
15. Jiang, Z.L., Yu H.R.: Experiments and development of long-test-duration hypervelocity detonation-driven shock tunnel (LHDst). AIAA 2014–1012 (2014)
16. He, D.: Wind Tunnel Balances. National Defence Industry Press, Beijing (2001). (in Chinese)
17. AIAA R-091-2003 Recommended Practice.: Calibration and use of internal strain-gage balances with application to wind tunnel testing. American Institute of Aeronautics and Astronautics, VA, USA (2003)
18. Cheng, H.K.: Hypersonic shock-layer theory of a yawed cone and other three-dimensional pointed bodies. WADC TN 59–335 (1959)
19. Ladson, C., Blackstock, T.: Air-helium simulation of the aerodynamic force coefficients of cones at hypersonic speeds. NASA TN D-1473 (1962)
20. Penland, J.A.: Aerodynamic force characteristics of a series of lifting cone and cone-cylinder configurations at $m = 6.83$ and angles of attack up to 130 degree. NASA TN D-840 (1961)